Proton disorder in cubic ice: effect on the electronic and optical properties

Garbuio, Viviana ; Cascella, Michele ; Kupchak, Igor ; Pulci, Olivia ; Seitsonen, Ari Paavo

Abstract: The proton disorder in ice has a key role in several properties such as the growth mode, thermodynamical properties, and ferroelectricity. While structural phase transitions from proton disordered to proton ordered ices have been extensively studied, much less is known about their electronic and optical properties. Here, we present ab initio many body perturbation theory-based calculations of the electronic and optical properties of cubic ice at different levels of proton disorder. We compare our results with those from liquid water, that acts as an example of a fully (proton- and oxygen-)disordered system. We find that by increasing the proton disorder, a shrinking of the electronic gap occurs in ice, and it is smallest in the liquid water. Simultaneously, the excitonic binding energy decreases, so that the final optical gaps result to be almost independent on the degree of proton disorder. We explain these findings as an interplay between the local dipolar disorder and the electronic correlation.

DOI: https://doi.org/10.1063/1.4929468

AIP | The Journal of Chemical Physics

Proton disorder in cubic ice: Effect on the electronic and optical properties

Viviana Garbuio, Michele Cascella, Igor Kupchak, Olivia Pulci, and Ari Paavo Seitsonen

Citation: The Journal of Chemical Physics **143**, 084507 (2015); doi: 10.1063/1.4929468
View online: http://dx.doi.org/10.1063/1.4929468
View Table of Contents: http://scitation.aip.org/content/aip/journal/jcp/143/8?ver=pdfcov
Published by the AIP Publishing

Proton disorder in cubic ice: Effect on the electronic and optical properties

Viviana Garbuio,[1] Michele Cascella,[2] Igor Kupchak,[3] Olivia Pulci,[1] and Ari Paavo Seitsonen[4,5]

[1]*MIFP, ETSF, Physics Department of Tor Vergata University, Via della Ricerca Scientifica 1, I-00133 Rome, Italy*

[2]*Department of Chemistry and Centre for Theoretical and Computational Chemistry (CTCC), University of Oslo, Postboks 1033, Blindern, N-0315 Oslo, Norway*

[3]*MIFP, V. Lashkarev Institute of Semiconductor Physics of National Academy of Sciences of Ukraine, pr. Nauki 45, UA-03680 Kiev, Ukraine*

[4]*Institut für Chemie, Universität Zürich, Winterthurerstrasse 190, CH-8057 Zürich, Switzerland*

[5]*Département de Chimie, École Normale Supérieure, 24 rue Lhomond, F-75005 Paris, France*

(Received 5 June 2015; accepted 11 August 2015; published online 27 August 2015)

The proton disorder in ice has a key role in several properties such as the growth mode, thermodynamical properties, and ferroelectricity. While structural phase transitions from proton disordered to proton ordered ices have been extensively studied, much less is known about their electronic and optical properties. Here, we present *ab initio* many body perturbation theory-based calculations of the electronic and optical properties of cubic ice at different levels of proton disorder. We compare our results with those from liquid water, that acts as an example of a fully (proton- and oxygen-)disordered system. We find that by increasing the proton disorder, a shrinking of the electronic gap occurs in ice, and it is smallest in the liquid water. Simultaneously, the excitonic binding energy decreases, so that the final optical gaps result to be almost independent on the degree of proton disorder. We explain these findings as an interplay between the local dipolar disorder and the electronic correlation. © *2015 AIP Publishing LLC.* [http://dx.doi.org/10.1063/1.4929468]

I. INTRODUCTION

The phase diagram of H_2O is probably the richest and most intriguing in nature. The large variety of structures of ice, its importance in many research fields, and the still open questions concerning the local structure of water and ice and its connection to their optical and X-ray spectra[1–13] make this system extremely interesting.

Ordinary water can solidify in 15 crystalline and several amorphous forms.[14] Among these, under mild temperature and pressure conditions ice has a hexagonal crystal structure with the oxygen atoms laying on a hexagonal wurtzite lattice and the hydrogens disordered but obeying Bernal-Fowler ice rules.[15] These rules state that each oxygen must be covalently bonded to two hydrogen atoms, and hydrogen bonded to two other hydrogen atoms. Moreover, there can be only one hydrogen atom per bond. The excited state properties of the hexagonal phase of ice (ice I_h) have been experimentally studied by Kobayashi.[16] Ice I_h is stable, at ambient pressure, down to about 72 K; below this temperature, a proton ordered ferroelectric phase, ice XI, becomes energetically more favorable.

At ambient pressure and temperatures between 113 and 153 K cubic ice (I_c), a metastable form, can be found. In this case, the sublattice of the oxygen atoms has a simple fcc diamond structure, while the hydrogens still obey to the Bernal-Fowler ice rules. Beyond fulfilling these rules, orientational disorder can be present and thus several different configurations are possible. Many physical quantities such as thermodynamical properties or ferroelectricity of the various ice phases depend on the eventual presence of this orientational disorder.

In this work we focus on ice I_c, investigating the electronic and optical properties of configurations at different levels of orientational order. We chose to investigate the ice I_c because it is more isotropic than ice I_h, thus simplifying the analysis and assignment of results to electronic effects only. In these ice systems structural[17–21] and electronic properties, such as band structures and dielectric constants,[21] have been studied within the density functional theory (DFT) approach. Infrared spectra of cubic ice have been recently experimentally measured and calculated within DFT.[22] Concerning the excited state properties of ice I_c, these have been experimentally probed many years ago by Watanabe.[23] From a theoretical point of view, these properties have been investigated within DFT[24] and tight binding methods,[25–27] but neither many-body effects have been included nor the effects of the proton disorder on these properties discussed in there.

Here, we analyze the influence of proton disorder on the electronic states and on the excitonic effects in ice I_c studying the fully proton-ordered polar structure and three other, proton-disordered ones. We also compare the properties of ice I_c with previous[28–30] and new results related to the most "disordered" phase, liquid water. We consider the different molecular orientations that lead both to a geometrical disorder and to a dipolar electrostatic disorder. We perform calculations of the electronic band structures and of the excitonic effects within many-body perturbation theory (MBPT) within the self-energy and Bethe-Salpeter approaches, that have already

shown their strength and predictive power (for a review, see, for example, Ref. 31).

Apart from realizing another step toward the complete comprehension of the H_2O properties, we will also indicate a new potential way to discriminate among proton ordered and proton disordered structures with spectroscopic characterization, opposed to traditional structural diffraction.

This paper is organized as follows: in Section II the theoretical methods are briefly described together with the details of the calculations. In Section III the results related to the condensed phases of ice I_c are presented, grouped into electronic and optical properties. These results are further compared with those obtained from liquid water. Conclusions are drawn in Section IV.

II. THEORETICAL METHODS AND CALCULATION DETAILS

In this work, we compute excited state properties in four configurations of cubic ice at different levels of proton disorder, and in liquid water. By disorder we here refer to the relative orientations of the dipole moments of the water molecules, not in the entropic or statistical sense. For ice I_c, we employ 8-molecule supercells with the hydrogens obeying the Bernal-Fowler ice rules. With 8 molecules, we can have four physically distinct configurations. These configurations have a degeneracy of 6, 12, 24, 48 and macroscopic polarization $\langle 100\rangle$, $\langle \frac{1}{2}\frac{1}{2}0\rangle$, $\langle 000\rangle$, and $\langle \frac{1}{2}00\rangle$, respectively.[17] We choose one of the possible structures in each case of polarization.

Out of the different dipole arrangements, in the apolar configuration ($\langle 000\rangle$) the orientation of the water molecules is the most proton-disordered one, leading to a total, or average dipole of zero, whereas in the other configurations there is more orientational ordering present. This point is important when we look at the microscopic local screening and at the excited state properties of these systems. In Table I, we show the local dipole orientation of each ice molecule and the average total dipole in all four considered structures. In practice, we evaluate the value and direction of the local dipole moments using the maximally localised Wannier functions from the DFT electronic structure.[32,33]

TABLE I. Orientation of dipoles of each H_2O molecule in ice 8-molecule supercell of I_c in the four symmetry-unique structures. On the second row, the total dipole moment per molecule $\overline{D}$ of each supercell is given. In the first column, the oxygen position of each of the 8 water molecules of the supercell is reported in relative units. The orientation of the dipoles of each molecule is given with triangles, empty and dotted spheres referring to left, right, into, and out of the plane, respectively.

Ice I_c model	$\langle 100\rangle$	$\langle \frac{1}{2}\frac{1}{2}0\rangle$	$\langle \frac{1}{2}00\rangle$	$\langle 000\rangle$
$\overline{D}$	1	$\frac{1}{\sqrt{2}}$	$\frac{1}{2}$	0
O = (0, 0, 0)	▷	△	⊙	▷
O = ($\frac{1}{2}$, $\frac{1}{2}$, 0)	▷	▷	◁	▷
O = ($\frac{1}{2}$, 0, $\frac{1}{2}$)	▷	△	▷	◁
O = (0, $\frac{1}{2}$, $\frac{1}{2}$)	▷	▷	⊙	◁
O = ($\frac{1}{4}$, $\frac{1}{4}$, $\frac{1}{4}$)	▷	▷	△	⊙
O = ($\frac{3}{4}$, $\frac{3}{4}$, $\frac{1}{4}$)	▷	△	▽	⊙
O = ($\frac{3}{4}$, $\frac{1}{4}$, $\frac{3}{4}$)	▷	▷	⊙	○
O = ($\frac{1}{4}$, $\frac{3}{4}$, $\frac{3}{4}$)	▷	△	⊙	○

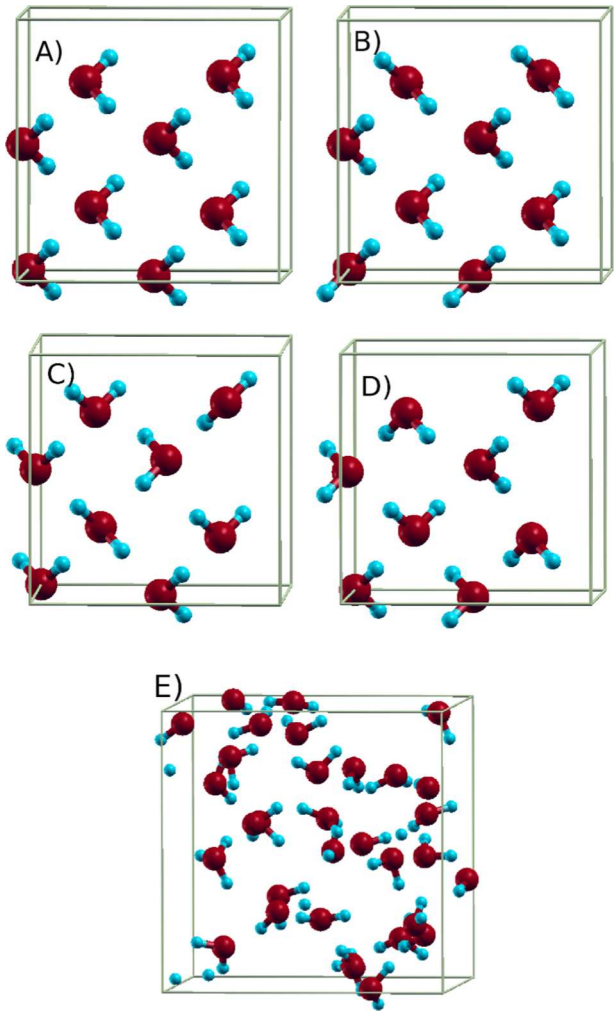

FIG. 1. Simulation cells of the four cubic ice models and liquid water. (a) Ice $I_c(\langle 100\rangle)$, (b) $I_c(\langle \frac{1}{2}\frac{1}{2}0\rangle)$, (c) $I_c(\langle \frac{1}{2}00\rangle)$, (d) $I_c(\langle 000\rangle)$, (e) one of the liquid water snapshots.

In this study, liquid water is the most disordered system, with both the hydrogens and the oxygens free of lattice constraints, but still forming a hydrogen bond network among the molecules. For the study of its excited state properties, we use the same strategy that was successfully tested in our previous work:[28] we perform classical molecular dynamics (MD) simulations with the TIP4P[50] water model and extract 20 snapshots from the trajectory.[34] Subsequently, we calculate the excited state properties in these configurations and average the results. In the present case, the water box includes 32 H_2O molecules with periodic boundary conditions imposed. The simulation cells of the four ice I_c models and liquid water are shown in Fig. 1.

For all ice systems and for liquid water, we perform electronic and spectroscopic calculations at three levels:

1. We start with DFT[35,36] to obtain the Kohn-Sham (KS) eigenvalues and eigenvectors.
2. In the second step, we correct the KS eigenvalues using the Green's function perturbation approach, within the GW approximation, where G is the single particle Green

function and W the screened Coulomb interaction.[37] In the following, we always refer to the GW energies, like energy gaps and densities of states (DOS), unless explicitly mentioned.

3. The excitonic binding energy and the optical gap are finally calculated by solving the Bethe-Salpeter equation (BSE),[31,51] fully including local-field effects and the electron-hole interaction.

Within the single-particle (i.e., DFT-RPA) approach we also calculate the macroscopic dielectric constant, ϵ_M, at two different levels of theory: with local field effects included (LF), that is, fully taking into account the microscopic inhomogeneity of the system through the evaluation of $\epsilon_m(\vec{r},\vec{r}')$, and without local fields included (NLF), hence approximating the microscopic dielectric function as $\epsilon_m(\vec{r},\vec{r}') \sim \epsilon_m(\vec{r}-\vec{r}')$, that neglects the inhomogeneity of the system. The macroscopic dielectric constant ϵ_M is thus obtained as either $\epsilon_M^{\mathrm{LF}} = 1/\left\{\left[\epsilon_{\vec{G}\vec{G}'}(q,\omega)\right]^{-1}\big|_{\vec{G},\vec{G}',q,\omega=0}\right\}$ or $\epsilon_M^{\mathrm{NLF}} = \epsilon_{\vec{G}\vec{G}'=0}(q=0,\omega=0)$, where $\vec{G}$ and $\vec{G}'$ are reciprocal lattice vectors, and q and ω are the transferred momentum and energy, respectively.

In all the DFT simulations we exploit the Quantum ESPRESSO code,[38,39] with generalized gradient approximation Perdew-Wang (GGA-PW91) exchange-correlation functional.[40] In the MBPT calculations, the exchange-correlation self-energy Σ is calculated within the G_0W_0 approximation ($\Sigma = iG_0W_0$, where G_0 is the one-particle Green's function and $W_0 = \epsilon^{-1}v$ is the screened Coulomb interaction).[31,37,41] In the last step, the solution of the Bethe-Salpeter equation, we use the `exc` code[42] and we adopt the Haydock algorithm[43] to avoid the direct diagonalization of the excitonic Hamiltonian.[44]

In the liquid water, we have previously demonstrated[28] that the GW corrections to the KS eigenvalues are almost identical in all the snapshots and that the same screened Coulomb potential $\epsilon_{\vec{G},\vec{G}'}(q,\omega)$ can be used for all the configurations; therefore, we calculate the ϵ^{-1} and the GW corrections only for one snapshot and apply them in the subsequent ones.

III. RESULTS AND DISCUSSION

A. Electronic properties

The DFT underestimation of the electronic gap between the valence and conduction bands is a well-known issue and is relevant also in our H_2O systems. In Fig. 2, we show the electronic gap of liquid water at the Γ point: in the left panel the DFT valence band maximum (VBM) and conduction band minimum (CBM) are reported at all the 20 MD snapshots, showing small variation (tenths of eV) in the value of the gap among the configurations. In the right panel, we show the average value of the VBM and CBM levels both within DFT and GW. The opening of the bandgap is evident when the self-energy contribution is included within the GW approximation.

The values of the electronic bandgaps in ice I_c and liquid water are reported in Table II. Three of the ice I_c structures have a direct electronic gap at Γ, with the only exception of configuration $I_c(\langle\frac{1}{2}00\rangle)$ that has an indirect X-Γ gap; it is, however, only 0.05 eV smaller that the direct one (which is located at Γ). We observe a clear trend: the gaps decrease with an increasing level of proton disorder, as expected, for example, in amorphous systems.[45] The trend is in agreement with the one seen previously in Ref. 21; the quantitative differences are probably due to fully relaxed structures in that work, whereas we used idealised geometries.

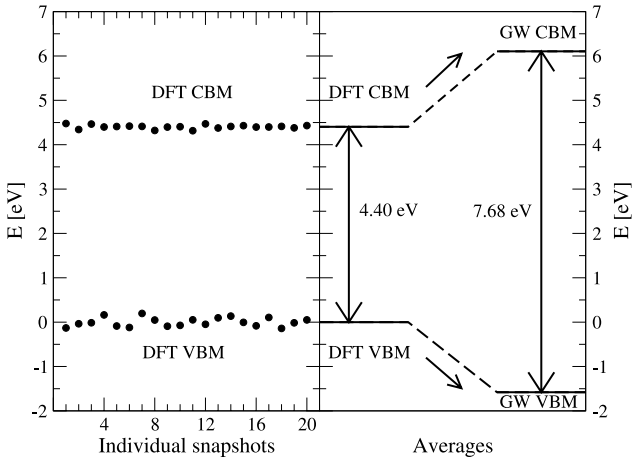

FIG. 2. Valence Band Maximum (VBM) and Conduction Band Minimum (CBM) of liquid water (32 molecules) at the Γ point. Left panel: the KS energy levels in the 20 chosen MD configurations. Right panel: the average values from the DFT and the GW calculations.

It is interesting to notice that the shrinking of the gap in structures with proton disorder is larger at the GW level than at the DFT one. We attribute this finding to the effects of the microscopic, dipolar electrostatic disorder: the larger the dipolar disorder, the smaller the electronic correlation and the screened potential W. The proton disorder does not, however, affect the long range electron-electron correlation, since the macroscopic dielectric functions ε_M (with or without LF) are practically the same in all cases (Table II).

We present in Fig. 3 the electronic band structure of ice I_c along high symmetry lines in the Brillouin zone. For more clarity, we show it only in two ice configurations: the most-dipole-ordered system $I_c(\langle 100\rangle)$ and the most-dipole-disordered $I_c(\langle 000\rangle)$. We observe a reduction of the electronic gap in the latter one, but small differences are also present in the deeper valence states. If we align band structures at the

TABLE II. DFT and GW electronic gaps at the Γ point, optical gaps and exciton binding energies (in eV) and the macroscopic electronic dielectric constant, calculated both with (LF) and without (NLF) local field effects. In the $I_c(\langle\frac{1}{2}00\rangle)$ configuration, the minimum electronic gap is indirect from X to Γ and its value is 5.65 eV at DFT and 9.08 eV at GW level.

	Ice I_c				
	$\langle 100\rangle$	$\langle\frac{1}{2}\frac{1}{2}0\rangle$	$\langle\frac{1}{2}00\rangle$	$\langle 000\rangle$	Liquid water
DFT gap	5.76	5.72	5.70	5.56	4.40
GW gap	9.5	9.2	9.1	9.0	7.7
Optical gap	7.5	7.4	7.4	7.5	7.2
Binding energy	2.0	1.8	1.7	1.5	0.5
ϵ_M^{LF}	1.94	1.94	1.94	1.93	2.07
$\epsilon_M^{\mathrm{NLF}}$	1.06	1.06	1.05	1.05	1.28

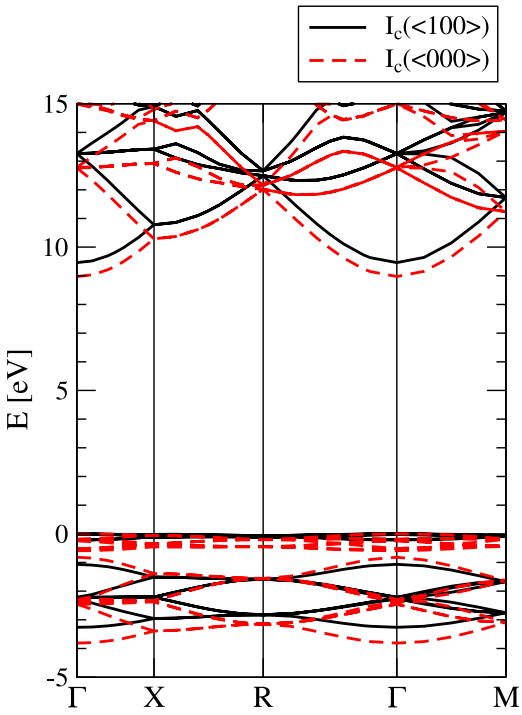

FIG. 3. Electronic band structure, calculated within the GW framework, in ice I$_c$(⟨100⟩) (continuous black lines) and ice I$_c$(⟨000⟩) (red dashed lines). Bands are aligned to the top of the VBM.

CBM, we see that the conduction bands are very similar in the two structures. The top eight bands of the valence band have a larger dispersion in I$_c$(⟨000⟩) than in I$_c$(⟨100⟩), partially explaining the reduction of the bandgap in the former.

Similarly, we show in Fig. 4 the total density of states (TDOS) and the projected DOS (PDOS) on the atomic orbitals of the H and O atoms at these two ice configurations. Both the TDOS and the PDOS in the proton ordered and disordered

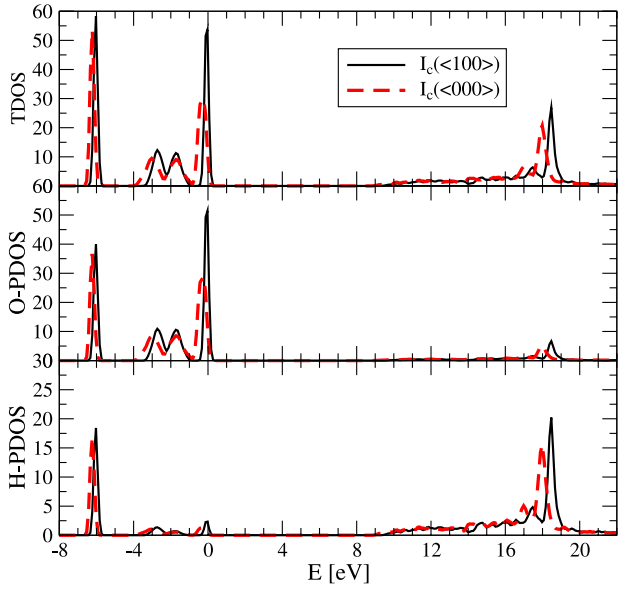

FIG. 4. GW DOSs of ice I$_c$(⟨100⟩) (black lines) and ice I$_c$(⟨000⟩) (red lines). Top panel: total densities of states (TDOS), O-PDOS (middle), and H-PDOS (bottom panel). Energies are aligned so that the TDOS due to VBM vanishes at zero. Gaussian broadening with $\sigma = 0.13$ eV was applied on the energy eigenvalues.

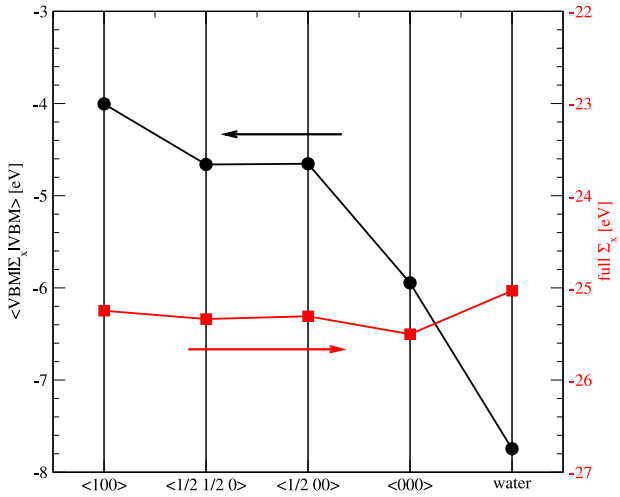

FIG. 5. Expectation value of the exchange part of the self-energy for increasing proton disorder. The red squares are correctly obtained summing over all the filled bands. The black circles are the values obtained considering only the VBM in the sum.

phases are very similar, and in general the features in the proton disordered phase are broadened, consistent with the larger dispersion in the band structure in the latter. The main difference is seen at high energies, where the peak mainly due to the H-s states is shifted.

For the gas-phase H_2O molecule and the liquid water dipole moments,[32,33] we find the (average) values of 1.75 D and 2.76 D, respectively, where the statistic fluctuation in the liquid is ±0.22 D.[46] In the cubic bulk ice, the dipole moment is 3.11 D at each H_2O molecule in all the configurations; this suggests that the effect of the solvation among the other molecules is large, but the relative orientation of the dipoles at the neighbouring molecules is irrelevant for the local dipole.

In order to understand better the effect of the proton disorder on the electronic structure, we have evaluated the

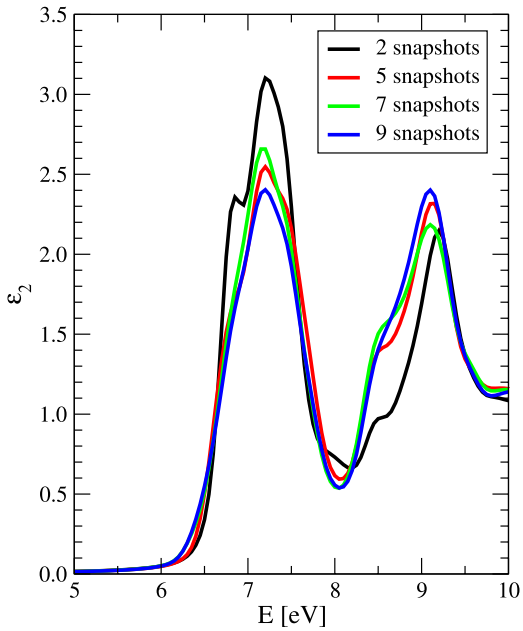

FIG. 6. Optical absorption spectrum of liquid water from the BSE approach obtained by averaging over an increasing number of snapshots (cf. Ref. 28).

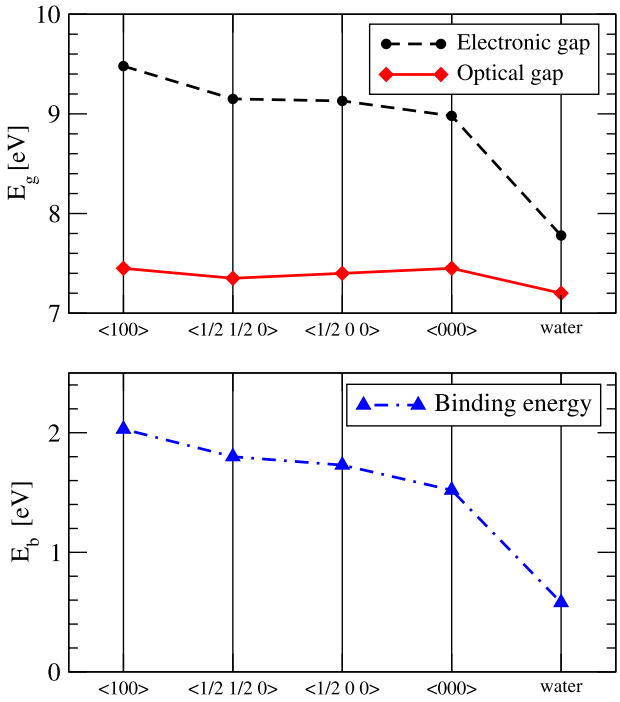

FIG. 7. GW electronic gap at the Γ point (black circles), optical gap (red diamonds), and excitonic binding energy (blue triangles) in the cubic ice structures and liquid water. Lines are guides for the eye.

electron localization function (ELF)[47] in the four ice systems. We show in Fig. S1 (please see the supplementary material[48]) the results in the same two ice cells as analysed above (the most proton-ordered, $I_c(\langle 100\rangle)$, and -disordered, $I_c(\langle 000\rangle)$). It is evident that the differences are negligible and thus the ELF does not provide us a way to explain the trends seen upon varying proton disorder. Hence, we decided to use an indirect method to analyze the electron localization at different degrees of proton disorder: we calculated what is the contribution of the highest occupied level to the exchange part of the self-energy, Σ_x. In other words, in the calculation of Σ_x, instead of summing over all the filled states we limit the sum only to the VBM state. These values are shown in Fig. 5 for all the systems studied. We find that the VBM contribution to the expectation value of Σ_x is quite important (around one fourth of the total summation) and varies significantly with orientational disorder: from −4.0 eV in ice $I_c(\langle 100\rangle)$ to −5.9 eV in ice $I_c(\langle 000\rangle)$, and to −7.7 eV in liquid water (see Fig. 5). This is a clear indication that the electronic wavefunction of the highest occupied band is more localized upon increasing proton disorder. Again this agrees well with the amount of band dispersion in the band structure, being the smallest in the most proton-ordered structure, or that the electronic states in this structure are most localised.

B. Optical properties

The inclusion of self-energy corrections and electron-hole interactions within the MBPT framework in the calculation of optical properties is essential in our case as already evidenced in previous works on similar systems;[24,28] in fact the first important feature in the optical spectrum, reported in the literature to reside in the range 8-9 eV in different aqueous systems,[16,23,24,49] does not get reproduced with single-particle approaches.[24]

In the calculations of the optical properties of liquid water, we limit the computation to only 9 MD snapshots. This choice, forced by the computational cost of the BSE simulations, can be validated by investigating the convergence of the average as a function of the number of considered configurations. In Fig. 6, we show the optical absorption spectra of liquid water obtained by averaging over an increasing number of snapshots and indeed only small differences are found.

In Table II, we report the values obtained in the four ice configurations and liquid water for the optical gap, here identified as the energy position of the maximum of the first excitonic peak, and the binding energy E_b which is defined as the difference between the electronic and optical gaps.

In all the systems there is a strongly bound exciton, with a binding energy decreasing from 2.0 eV in the most dipole-ordered phase to 1.6 eV in the most proton-disordered one. The binding energy in liquid water is much lower, with a value of 0.5 eV. The reduction in the exciton binding energy with increasing proton disorder is related to the reduction of the electron-hole interaction. These differences in the exciton binding energies counterbalance the corresponding differences in the electronic quasi-particle gaps, and as a result the optical gaps are almost independent of the local dipole disorder. This trend is seen in Fig. 7, where these values are plotted in the order of decreasing average total dipole (that is, increasing local dipolar disorder).

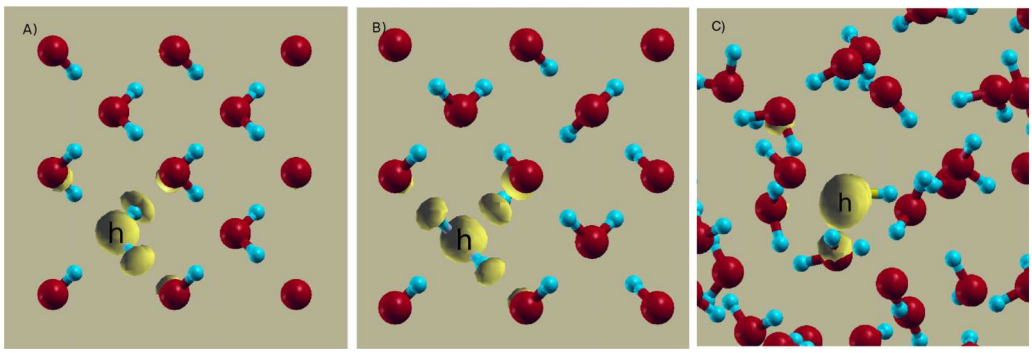

FIG. 8. Plot of the excitonic wavefunction in (a) ice $I_c(\langle 100\rangle)$, (b) ice $I_c(\langle 000\rangle)$, and (c) in one snapshot of liquid water. The symbol "h" indicates the oxygen atom at which the hole is fixed.

From the values of the macroscopic dielectric constant in Table II, we see that the local field effects are important in the ice and liquid water since the values of ϵ_M^{LF} and $\epsilon_M^{\mathrm{NLF}}$ differ nearly by a factor of two. On the other hand, both at either NLF or LF level, the value is practically the same in all the ice structures considered. From the negligible variation in ϵ_M, we conclude that the macroscopic averages of the electronic polarizability are the same, and the differences in the electronic and optical properties are due to the short- and intermediate-range variations in the dipolar disorder.

We investigate the variation in the excitonic wavefunction between different structures, focusing on the states contributing most to the first bound exciton. We fix the hole on an oxygen atom (identified in the pictures with an "h") and look at the electronic probability distribution. The plots of the excitonic wavefunctions are reported in Fig. 8 in two ice systems and in liquid water. We see that the electron-hole pair is mainly localized on the H_2O molecule on which the hole is fixed, and partially on the first neighbouring molecules. We confirmed that a slight shift of the hole toward the maximum of the O-p_z orbital or using a larger, $3 \times 3 \times 3$, cell does not change these conclusions. This finding supports the conclusion above drawn from the small variations in the macroscopic dielectric function: since the electron-hole interaction is practically limited to the first shell of neighbouring molecules, only the short range orientational order/disorder affects the electron-hole binding energy.

IV. CONCLUSIONS

In conclusion, we have calculated, within MBPT, the electronic and optical properties of cubic ice in a fully proton-ordered and polar structure, an apolar configuration, and two intermediate cases. We have compared the results at this varying level of proton disorder and also in liquid water, the latter acting as an example of an entirely (proton- and oxygen-) disordered system. We have focused on the geometrical disorder and in particular on the electrostatic disorder due to different molecular dipole orientations.

We find that upon increasing proton disorder, an expected shrinking of the electronic DFT gap appears. This effect is strengthened by the self-energy corrections, or moving from the DFT to the GW gap. Simultaneously, the exciton binding energy decreases also. We attribute the reduction in both the electronic gap and the exciton binding energy to the effects of the local dipolar disorder in the screened potential W: the larger the electrostatic disorder, the smaller the electronic correlation and hence W. The simultaneous decrease of the electronic gap and of the exciton binding energy counterbalances each other so that the final optical gaps result to be almost independent on the degree of proton disorder. Nevertheless, from an accurate measurement of the excitonic binding energies, and/or of the electronic gaps, it would be possible to discriminate among proton-ordered and -disordered structures.

When we study the excitonic wavefunction and fix the hole on one molecule, the electronic probability of the exciton is localized at the molecule on which the hole is fixed and on the first shell of neighbouring molecules in both ice and liquid waters. Also the macroscopic dielectric function, related to the long-range screening, remains almost constant despite the changing proton disorder. Therefore, we conclude that only the short range orientational order/disorder, due to the different local dipole orientations, has important effects on the excited state properties.

ACKNOWLEDGMENTS

We thank Lucia Reining for valuable scientific discussions. CPU time was granted from CINECA and ENEA-CRESCO. Fundings from EC project IRSES SIMTECH (No. GA 246937) are gratefully acknowledged. M.C. acknowledges the support of the Norwegian Research Council through the CoE Centre for Theoretical and Computational Chemistry (CTCC) Grant Nos. 179568/V30 and 171185/V30.

[1]J. D. Smith, C. D. Cappa, K. R. Wilson, B. M. Messer, R. C. Cohen, and R. J. Saykally, Science **306**, 851 (2004).
[2]A. K. Soper, Pure Appl. Chem. **1855**, 82 (2010).
[3]B. Heténi, F. De Angelis, P. Giannozzi, and R. Car, J. Chem. Phys. **120**, 8632 (2004).
[4]M. Iannuzzi, J. Chem. Phys. **128**, 204506 (2008).
[5]D. Prendergast and G. Galli, Phys. Rev. Lett. **96**, 215502 (2006).
[6]T. Head-Gordon and M. E. Johnson, Proc. Natl. Acad. Sci. U. S. A. **103**, 7973 (2006).
[7]T. Head-Gordon and S. W. Rick, Phys. Chem. Chem. Phys. **9**, 83 (2007).
[8]G. Brancato, N. Rega, and V. Barone, Phys. Rev. Lett. **100**, 107401 (2008).
[9]W. Chen, X. Wu, and R. Car, Phys. Rev. Lett. **105**, 017802 (2010).
[10]A. Nilsson and L. G. M. Pettersson, Chem. Phys. **389**, 1 (2011).
[11]L. B. Skinner, C. Huang, D. Schlesinger, L. G. M. Pettersson, A. Nilsson, and C. J. Benmore, J. Chem. Phys. **138**, 074506 (2013).
[12]L. Kong, X. Wu, and R. Car, Phys. Rev. B **86**, 134203 (2013).
[13]A. K. Soper, ISRN Phys. Chem. **2013**, 279463.
[14]C. G. Salzmann, P. G. Radaelli, E. Mayer, and J. L. Finney, Phys. Rev. Lett. **103**, 105701 (2009).
[15]J. D. Bernal and R. H. Fowler, J. Chem. Phys. **1**, 515 (1933).
[16]K. Kobayashi, J. Phys. Chem. **87**, 4317 (1983).
[17]C. Lee, D. Vanderbilt, K. Laasonen, R. Car, and M. Parrinello, Phys. Rev. B **47**, 4863 (1993).
[18]C. Czaplewski, "Simulation of the crystal structure of ice," Technical Report EPCC-SS96-02 (Faculty of Chemistry, University of Gdańsk, Poland, 1996).
[19]S. Casassa, M. Calatayud, K. Doll, C. Minot, and C. Pisani, Chem. Phys. Lett. **409**, 110 (2005).
[20]Z. Raza, D. Alfè, C. G. Salzmann, J. Klimeš, A. Michaelides, and B. Slater, Phys. Chem. Chem. Phys. **13**, 19788 (2011).
[21]S. Wang, Int. J. Quantum Chem. **113**, 661 (2013).
[22]P. Geiger, C. Dellago, M. Macher, C. Franchini, G. Kresse, J. Bernard, J. N. Stern, and T. Loerting, J. Phys. Chem. C **118**, 10989 (2014).
[23]M. Watanabe, H. Kitamura, and Y. Nakai, in *Proceeding of IVth International Conference on VU Radiation Physics* (Pergamon, New York, 1974), p. 70.
[24]W. Y. Ching, L. Liu, and Y. N. Xu, Ferroelectrics **153**, 25 (1994).
[25]L. Resca and R. Resta, Phys. Status Solidi B **81**, 129 (1977).
[26]G. Pastori Parravicini and L. Resca, J. Phys. C: Solid State Phys. **4**, L314 (1971).
[27]G. Pastori Parravicini and L. Resca, Phys. Rev. B **8**, 3009 (1973).
[28]V. Garbuio, M. Cascella, L. Reining, R. Del Sole, and O. Pulci, Phys. Rev. Lett. **97**, 137402 (2006).
[29]V. Garbuio, M. Cascella, and O. Pulci, J. Phys.: Condens. Matter **21**, 033101 (2009).
[30]C. Fang, W.-F. Li, R. S. Koster, J. Klimeš, A. van Blaaderen, and M. A. van Huis, "The accurate calculation of the band gap of liquid water by means of GW corrections applied to plane-wave density functional theory molecular dynamics simulations," Phys. Chem. Chem. Phys. **17**, 365 (2015).
[31]G. Onida, L. Reining, and A. Rubio, Rev. Mod. Phys. **74**, 601 (2002).
[32]P. L. Silvestrelli and M. Parrinello, Phys. Rev. Lett. **82**, 3308 (1999).
[33]P. L. Silvestrelli and M. Parrinello, Phys. Rev. Lett. **82**, 5415 (1999).
[34]We sampled every 2 ns a 40 ns long classical MD simulation trajectory. This run was done in the NVT ensemble, applying a Nosé-Hoover thermostat. The TIP4P water model[50] has been used to represent the water

molecules in our simulation box. Electrostatic interactions were treated using the particle mesh Ewald method and all van der Waals interactions between non-bonded atom pairs were included.
[35]P. Hohenberg and W. Kohn, Phys. Rev. **136**, B864 (1964).
[36]W. Kohn and L. J. Sham, Phys. Rev. **140**, A1133 (1965).
[37]L. Hedin, Phys. Rev. **139**, A796 (1965).
[38]P. Giannozzi *et al.*, J. Phys.: Condens. Matter **21**, 395502 (2009).
[39]In the ice systems we use a cubic 8-molecule supercell, a kinetic energy cutoff of 60 Ry, and 500 empty states, and we sample the whole Brillouin zone with 64 k-points. We fix the geometry of the molecules at $d_{OH} = 0.963$ Å and $\angle_{HOH} = 109.52°$ and the lattice constant at 6.350 Å. In calculations on liquid water, we have MD snapshots with 32 H_2O molecules in a cubic unit cell with the length of 9.671 Å. We use a kinetic energy cutoff of 50 Ry, and 600 empty energy levels, and we sample the full Brillouin zone with 8 k-points.
[40]J. P. Perdew, J. A. Chevary, S. H. Vosko, K. A. Jackson, M. R. Pederson, D. J. Singh, and C. Fiolhais, Phys. Rev. B **46**, 6671 (1992).
[41]In all the studied systems, the screened Coulomb interaction $\epsilon^{-1}v$ is calculated in the plasmon pole approximation and the self-energy corrections within the first order perturbation theory. In the two ice configurations, we use 2517 plane waves for the calculation of the ϵ^{-1} and of the correlation part of the self-energy (Σ_C) and 14 939 plane waves for the exchange part of the self-energy (Σ_X). In the liquid water snapshots, we use 13 997 plane waves in the calculation of ϵ^{-1}, 10 059 plane waves for Σ_C, and 29 039 plane waves for Σ_X.
[42]The EXC code v3.1 is available at http://www.Bethe-Salpeter.org/ under the GNU Public License (https://gnu.org/licenses/licenses.en.html#GPL).
[43]R. Haydock, Comput. Phys. Commun. **20**, 11 (1980).
[44]For the solution of the Bethe-Salpeter equation, we adopt the resonant approximation.[51] In the two ice configurations we consider 24 valence states, 38 conduction states, and we perform 150 iterations in the Haydock algorithm. In the liquid water snapshots, we consider 96 valence states, 120 conduction states, and we perform 200 iterations in the Haydock algorithm.
[45]M. A. Kanehisa and R. J. Elliott, Phys. Rev. B **35**, 2228 (1987).
[46]This value is lower than the ones usually seen in the literature with corresponding computational setup due to the specific, fixed intramolecular geometry used and the simulated trajectory that was done here employing the TIP4P force field.
[47]A. D. Becke and K. E. Edgecombe, "A simple measure of electron localization in atomic and molecular systems," J. Chem. Phys. **92**, 5397 (1990).
[48]See supplementary material at http://dx.doi.org/10.1063/1.4929468 for contains the figures of the electron localisation function in two different configurations of ice.
[49]G. D. Kerr, R. N. Hamm, M. W. Williams, R. D. Birkhoff, and L. R. Painter, Phys. Rev. A **5**, 2523 (1972).
[50]W. L. Jorgensen and J. D. Madura, "Temperature and size dependence for Monte Carlo simulations of TIP4P water," Mol. Phys. **56**, 1381 (1985).
[51]A. L. Fetter and J. D. Walecka, *Quantum Theory of Many-Particle Systems* (McGraw-Hill, New York, 1971).